Interaction of a large amplitude interfacial solitary wave of depression with a bottom step

Vladimir Maderich,[1] Tatiana Talipova,[2] Roger Grimshaw,[3] Katherina Terletska,[1] Igor Brovchenko,[1] Efim Pelinovsky,[2] and Byung Ho Choi[4]
[1]*Department of Marine and River Systems, Institute of Mathematical Machine and System Problems, 42 Glushkov Pr., 03187 Kiev, Ukraine*
[2]*Department of Nonlinear Geophysical Processes, Institute of Applied Physics, 46 Uljanov Street, 603950 Nizhny Novgorod, Russia*
[3]*Department of Mathematical Sciences, Loughborough University, Loughborough LE11 3TU, United Kingdom*
[4]*Department of Civil and Environmental Engineering, Sungkyunkwan University, 440-746 Suwon, Republic of Korea*

(Received 3 December 2009; accepted 28 May 2010; published online 14 July 2010)

This paper is devoted to the study of the transformation of a finite-amplitude interfacial solitary wave of depression at a bottom step. The parameter range studied goes outside the range of weakly nonlinear theory (the extended Korteweg–de Vries or Gardner equation), and we describe various scenarios of this transformation in terms of the incident wave amplitude and the step height. The dynamics and energy balance of the transformation are described. Several numerical simulations are carried out using the nonhydrostatic model based on the fully nonlinear Navier–Stokes equations in the Boussinesq approximation. Three distinct runs are discussed in detail. The first simulation is done when the ratio of the step height to the lower layer thickness after the step is about 0.4 and the incident wave amplitude is less than the limiting value estimated for a Gardner solitary wave. It shows the applicability of the weakly nonlinear model to describe the transformation of a strongly nonlinear wave in this case. In the second simulation, the ratio of the step height to the lower layer thickness is the same as that in the first run but the incident wave amplitude is increased and then its shape is described by the Miyata–Choi–Camassa solitary wave solution. In this case, the process of wave transformation is accompanied by shear instability and the billows that result in a thickening of the interface layer. In the third simulation, the ratio of the step height to the thickness of the lower layer after the step is 1.33, and then the same Miyata–Choi–Camassa solitary wave passes over the step, it undergoes stronger reflection and mixing between the layers although Kelvin–Helmholtz instability is absent. The energy budget of the wave transformation is calculated. It is shown that the energy loss in the vicinity of the step grows with an increase of the ratio of the incident wave amplitude to the thickness of the lower layer over the step. © *2010 American Institute of Physics*. [doi:10.1063/1.3455984]

I. INTRODUCTION

A two-layer representation of the ocean density stratification is a useful approximation to apply analytical and numerical methods for the study of internal solitary waves. Rigorous mathematical proofs of the existence and properties of an interfacial solitary wave were found by Amick and Turner[1] and by Tung *et al.*[2] For small wave amplitudes, the dynamics of long interfacial solitary waves can be described using the extended Korteweg–de Vries or Gardner equation, which is an integrable equation.[3–6] In particular, as the wave amplitude is increased to a limiting value, its width is also increased and the limiting solitary wave has a "table-top" shape. The same properties are obtained using the Miyata, Choi–Camassa, and Ostrovsky–Grue models for strongly nonlinear but weakly dispersive solitary waves,[7–10] but these strongly nonlinear models predict a different value for the limiting wave amplitude. Some rigorous results have been obtained for internal large-amplitude solitary waves in a fluid with continuous density stratification using the conjugate flow approach.[11,12] Numerical calculations in the framework of the full Euler equations confirm the conclusions of these analytical theories.[13–15]

The effects of slowly varying bottom depth can be incorporated into these analytical theories and the transformation of a solitary wave over variable depth has been investigated in detail in both the weakly nonlinear approximation[16–21] and in the fully nonlinear model.[22] The case when the bottom topography varies rapidly is more difficult for theoretical analysis. Nevertheless, the transformation of a weakly nonlinear solitary wave at a bottom step seems to be quite well described in the framework of a weakly nonlinear asymptotic theory (see Ref. 23). In this paper, it is shown that in the vicinity of the step the wave transformation can be described using the linear long-wave theory for interfacial waves, from which the coefficients for wave reflection and transmission are calculated. The reflected and transmitted waves in the vicinity of a step have solitary-wave shapes, but their parameters do not satisfy the steady-state solution. Hence, they fission into secondary waves (internal solitons), and the use

of inverse scattering technique allows for an estimate of the number and amplitudes of these secondary solitons. For moderate and large incident wave amplitudes, this process has been studied numerically in the recent paper by Maderich *et al.*,[24] which considered the case when the interface was close to the bottom, and hence the incident wave was a wave of elevation. In these numerical experiments, the ratio of the initial wave amplitude to the layer thickness is varied up to one-half, and nonlinear effects are then essential. In general, the characteristics of the generated solitary waves obtained in the fully nonlinear simulations are in reasonable agreement with the predictions of the theoretical model of Grimshaw *et al.*,[23] which is based on matching linear shallow-water theory in the vicinity of the step with solutions of the Gardner equation for waves far from the step.

In the present paper, the problem considered is that when the interface is close to the surface, and hence the incident interfacial solitary wave is a wave of depression. We pay particular attention to the effects of mixing, Kelvin–Helmholtz (KH) instability, and wave energy dissipation. The KH instability of parallel stratified flows is well studied experimentally, theoretically, and numerically (see, e.g., Refs. 25–28). An increase of shear in the progressive interfacial wave crest or trough also can result in KH instability.[29,30] It is important to mention that KH instability of large amplitude solitary waves in the layered fluid has been clearly observed in laboratory experiments in tanks of constant depth[13,31,32] and has also been studied theoretically[33] and modeled numerically in the framework of the Navier–Stokes equations.[34] Similar phenomena are observed in the ocean when the stratification is real.[35,36] The manifestation of such effects when a large amplitude solitary wave interacts with a bottom step has some specific features which we shall describe in this paper. We consider here the case when the incident wave is a depression interfacial solitary wave because its interaction with a bottom step and the consequent energy dissipation due to mixing is better pronounced than for an elevation interfacial solitary wave.

Theoretical formulas for interfacial solitary waves of moderate and large amplitudes are presented in Sec. II. Then the setup of nonhydrostatic numerical model for a stratified fluid is given in Sec. III, whereas the model is briefly described in the Appendix. The numerical results for the transformation of an interfacial depression solitary wave interacting with a bottom step are presented in Sec. IV. The energy dissipation due to these processes is discussed in Sec. V. Our results are summarized in Sec. VI.

II. ANALYTICAL MODELS FOR INTERFACIAL SOLITARY WAVES

The configuration for a two-layer stratification is shown in Fig. 1, where the upper and lower layers have thicknesses h_1 and h_2 with total depth $H=h_1+h_2$, and the densities ρ_1 and ρ_2, respectively. The difference between densities, $\Delta\rho=\rho_2-\rho_1$, is assumed to be small compared to either undisturbed density ρ_0, that is, we use the Boussinesq approximation. The interface lies near the surface ($h_1<h_2$) and as is well-known, the solitary wave has negative polarity, and so is a wave of depression. A solitary wave with the interface displacement $\eta(x,t)$ approaches the bottom step from the right. For convenience, we say that the incident wave approaches from deep to shallow water but, of course, both depths are smaller the wavelength. The thickness of lower layer before the step is h_{2-} and after the step is h_{2+}.

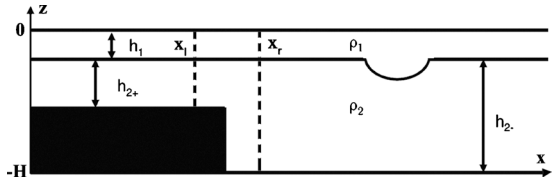

FIG. 1. Sketch of the problem. Dashed lines shows cross sections where energy fluxes are calculated (see Sec. V).

The analytical description of interfacial solitary waves of weak and moderate amplitudes can be carried out using the extended Korteweg–de Vries (Gardner) equation[3–5]

$$\frac{\partial\eta}{\partial t}+(c_0+\alpha\eta+\alpha_1\eta^2)\frac{\partial\eta}{\partial x}+\beta\frac{\partial^3\eta}{\partial x^3}=0, \tag{1}$$

where t is time and x is the horizontal coordinate. The coefficients of Eq. (1) are (in the Boussinesq approximation)

$$c_0=\sqrt{g\frac{\Delta\rho}{\rho_0}\frac{h_1h_2}{h_1+h_2}}, \tag{2}$$

$$\alpha=\frac{3c_0}{2}\frac{h_1-h_2}{h_1h_2},\quad \beta=\frac{c_0h_1h_2}{6}, \tag{3}$$

$$\alpha_1=-\frac{3c_0}{8h_1^2h_2^2}(h_1^2+h_2^2+6h_1h_2).$$

Here c_0 is the linear long-wave phase speed of an interfacial wave, g is the gravity acceleration, and α, α_1, and β describe the coefficients of quadratic and cubic nonlinearity and dispersion, respectively. The steady-state solution of the Gardner equation describing the interface solitary wave is

$$\eta(x,t)=\frac{D}{1+B\cosh[\gamma(x-Vt)]}, \tag{4}$$

where

$$D=\frac{6\beta\gamma^2}{\alpha},\quad B^2=1+\frac{6\alpha_1\beta\gamma^2}{\alpha^2},\quad V=\beta\gamma^2, \tag{5}$$

and γ is a free parameter, inverse to the solitary wavelength. The solitary wave amplitude is

$$a=\frac{D}{1+B}, \tag{6}$$

and its sign is negative if $h_1/h_2<1$ (wave of depression). The wave amplitude varies from small values (where the Gardner equation coincides with the Korteweg–de Vries equation) to the limiting amplitude

$$a_{\lim} = -4h_1h_2\frac{h_2-h_1}{h_1^2+h_2^2+6h_1h_2}, \tag{7}$$

when the solitary wave has a table-top shape.

The Miyata–Choi–Camassa (MCC) equations describe the shallow-water solitary waves (MCC solitary waves) in the approximation of weak dispersion but with no limitation of nonlinearity (see Refs. 7–9). The shape of the solitary wave of amplitude a is determined from the ordinary nonlinear equation for the interfacial displacement η (in the Boussinesq approximation)

$$\left(\frac{d\eta}{dX}\right)^2 = \left[\frac{3c_0^2}{c^2h_1h_2(h_1-h_2)}\right] \times \frac{\eta^2(\eta-b_1)(\eta-b_2)}{(\eta-b_*)}, \tag{8}$$

where $X=x-ct$, and

$$b_* = \frac{h_1h_2}{h_2-h_1}, \quad c = c_0\sqrt{\frac{(h_1-a)(h_2+a)}{h_1h_2}}, \tag{9}$$

and the parameters b_1 and b_2 are the roots of the quadratic algebraic equation

$$b^2+q_1b+q_2=0, \tag{10}$$

where

$$q_1 = h_2-h_1, \quad q_2 = h_1h_2\left(\frac{c^2}{c_0^2}-1\right). \tag{11}$$

The implicit solution $X=X(\eta)$ may be obtained by integrating Eq. (8) and it is a combination of elliptic integrals.[9] The amplitude of the solitary wave varies from zero to the limiting value $A_{\lim}$,

$$A_{\lim} = \frac{h_1-h_2}{2}. \tag{12}$$

If the difference between the thicknesses of both layers is weak, the formula (12) coincides with the Gardner model formula (7). For large amplitudes, formula (12) predicts a larger value for the limiting solitary wave amplitude than Eq. (7).

To describe our numerical results, two parameters are introduced. The parameter of nonlinearity $\varepsilon_{\rm nl}=\alpha a/c_0+|\alpha_1|a^2/c_0$ in the weakly nonlinear asymptotic theory (the Gardner equation) characterizes the waves above a flat bottom. Strictly speaking, it should be much less than unity for applicability of the Gardner model. Nevertheless, in practice this model may be used even for $\varepsilon_{\rm nl}\geq 1$ (see Refs. 10 and 24). Another parameter $\mu=|a_-|/h_{2+}$ (see Ref. 37) characterizes the interaction of the wave with the step. Here a_- is the amplitude of the incident wave before the step and h_{2+} is the height of the lower layer over the step. The limit $\mu\to 0$ means that wave amplitude is small and $\mu=1$ when the incident wave amplitude is equal to the height of the lower layer and the disturbed interface touches the step. The numerically computed waves are compared with the analytical solutions of the Gardner and MCC equations.

III. NUMERICAL MODEL BASED ON THE NAVIER–STOKES EQUATIONS

The numerical model using the Navier–Stokes equations is fully described in Ref. 24 and briefly in the Appendix. It is applied here in a two-dimensional mode with the horizontal coordinate x and the vertical coordinate z (see Fig. 1). The computational tank parameters are as follows. The total length is 30 m, while the length of the deep part is 16 m and the step position is at $x=14$ m. The background stratification in the flume is modeled by two layers with upper and bottom layer salinities $S_{\rm up}=2$ and $S_{\rm bot}=15$ at constant temperature of 20 °C, respectively. The density jump $\Delta\rho/\rho_0$ is equal to 0.01. The vertical profile $S(z)$ in the transition zone is approximated by

$$S(z) = \frac{S_{\rm up}+S_{\rm bot}}{2} - \frac{S_{\rm bot}-S_{\rm up}}{2}\tanh\left[\frac{(z-h_1)}{dh}\right], \tag{13}$$

where the interface initial thickness for $dh=0.2$ cm is much less than the thickness of both layers. In the simulations, we visualize the interface as an isohaline with salinity equal to 8.5, which is located at $z=h_1$. All runs are carried out with the thickness of the upper layer $h_1=4$ cm and thickness of lower layer in the deeper part of tank $h_{2-}=28$ cm. The height of the step is varied between 8 cm for runs 1 and 2 and 16 cm for run 5. The numerical experiments are carried out with molecular values of kinematic viscosity $\nu=1.14\times10^{-6}$ m^2 s^{-1} and diffusivity of salt $\chi=10^{-9}$ m^2 s^{-1}. Nonslip boundary conditions at the bottom and end walls are used, whereas at the free surface the viscous stresses are set to zero. The flux of salinity through the flume boundaries is also set to zero. Essentially a computational grid 2400 $\times$120 is used, but for runs 2 and 5 grids 4800$\times$240 and 9600$\times$480 are also used to verify effect of grid resolution on the wave transformation and do make the fine structure clearer. In the numerical experiments, the solitary wave is generated by a collapse of mixed volume at the right-end side of the tank. Further details of the method are described by Maderich *et al.*[24]

TABLE I. The parameters of runs.

Run	h_{2+} (cm)	a_- (cm)	h_{2+}/h_{2-}	a_-/h_1	$a_-/a_{\lim-}$	$a_-/A_{\lim-}$	$\varepsilon^-_{\rm nl}$	μ
1	20	−6.6	0.71	1.65	0.90	0.55	4.0	0.33
2	20	−8.8	0.71	2.2	1.2	0.74	6.5	0.44
3	17.6	−8.8	0.63	2.2	1.2	0.74	6.5	0.5
4	14.7	−8.8	0.53	2.2	1.2	0.74	6.5	0.6
5	12	−8.8	0.43	2.2	1.2	0.74	6.5	0.73

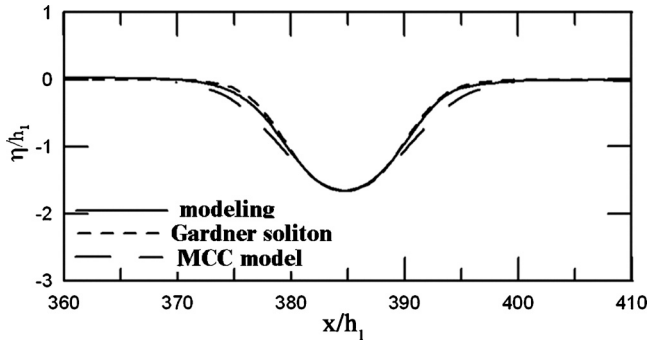

FIG. 2. The comparison of the incident solitary wave shape before the step at $\tau=276$ with the shape of Gardner and MCC solitary waves in run 1.

Note that we use analytical two-layer models, meanwhile in experiment there is continuous stratification. The coefficients of the Gardner model are calculated using the density ratio $\Delta\rho/\rho_0$ and an interface position of $z=h_1$ as indicated above. The difference in the computed coefficients of the Gardner equation between a two-layer and a continuous stratification does not exceed a few percent. Hence, the theory developed for our two-layer model can be applied for explanation of results for the continuous stratification.

IV. NUMERICAL SIMULATIONS OF WAVE TRANSFORMATION AT A STEP

We present our results in a dimensionless form where the horizontal x and vertical z coordinates and interface displacement η are normalized on the height of the upper layer h_1 and time t is normalized to τ by

$$\tau = t/\sqrt{\rho_0 h_1/(\Delta\rho g)}. \tag{14}$$

This allows us to apply the results to an oceanic situation using appropriate scaling. The input parameters of runs are presented in Table I. Here and in the sequel − and + denote values of variables before and after step, respectively. The characteristics of incident solitary waves in Table I are estimated in the vicinity of the step at the cross section $x_r = 14.2$ m (Fig. 1). To estimate the nonlinearity of the interfacial solitary wave, we calculate the limiting values of the solitary wave amplitude according to the Gardner equation $a_{\lim}$ [Eq. (7)] and Camassa–Choi theory $A_{\lim}$ [Eq. (12)], and they are also given in Table I. Three qualitatively distinct runs (1, 2, and 5) are analyzed in detail below.

A. Run 1

Near the step (at x_r), the incident wave amplitude is equal to −6.6 cm and its shape is well described by both the Gardner and MCC models [Figs. 2 and 3(a)]. Nevertheless, the MCC solitary wave is a little bit wider. The "interaction" parameter is small for this run ($\mu=0.33$) and we assume that the Gardner equation theory may be applied to describe the reflection and transmission of this incident wave.[23] The reflection coefficient R from the step computed using the formula from linear theory[23,24] $R=(1-c_+/c_-)/(1+c_-/c_+)$ is very small and it is equal to 0.01. This is why reflection is not visible in Fig. 3(b). The transmission coefficient according to the linear theory is $T=2/(1+c_+/c_-)$ and it is equal to 1.01.

The transmitted wave amplitude immediately after the step equals −6.7 cm [Fig. 3(b)], coinciding with "linear" predicted amplitude Ta_-. There is no wave disturbance at the step and there is no transformation of energy due to any instability. Then, the transmitted pulse transforms into a solitary wave and a weak oscillatory tail [Fig. 3(d)]. The amplitude of the transmitted solitary wave is −5.1 cm and it is 24% less than on a step (Fig. 4).

It should be noted here that the transmitted wave is almost the same as the incident wave because the reflection coefficient is only 1%; nevertheless, it transforms strongly in the left-hand side of tank. There is a noticeable change in nonlinearity (more than 10%) and a large changing in disper-

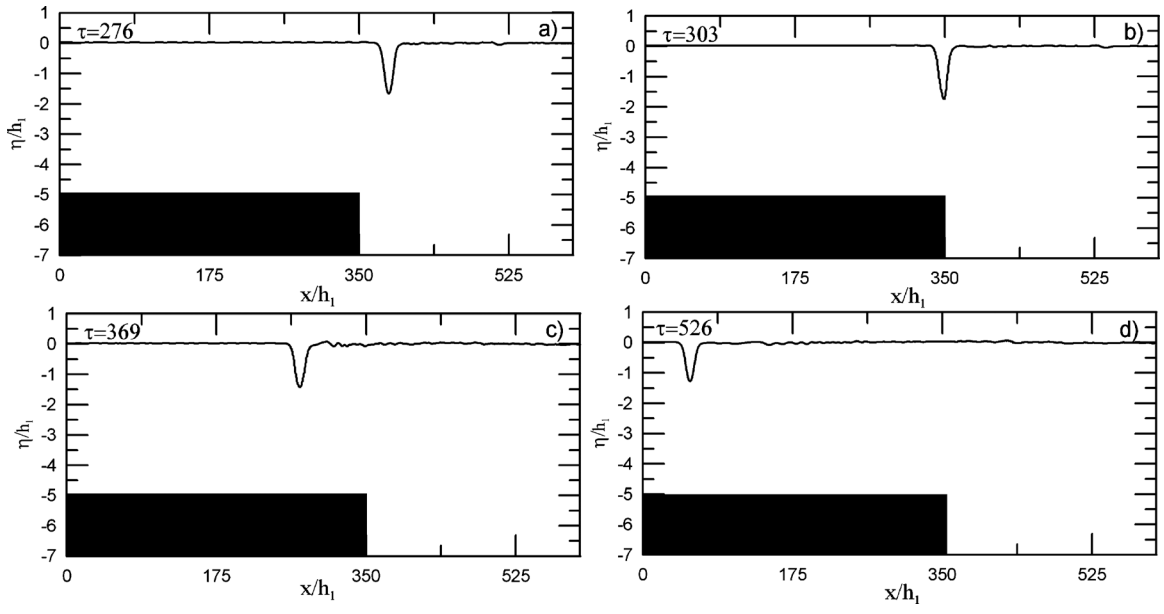

FIG. 3. Solitary wave transformation at the step in run 1 at successive times.

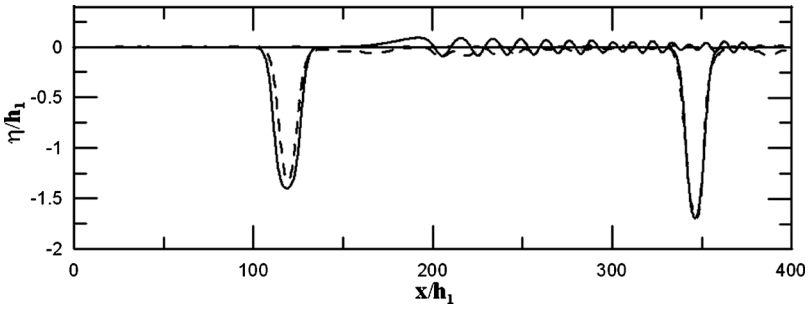

FIG. 4. The comparison of the solitary wave transformation after step in the Gardner model (solid line) and full nonlinear model (dashed line) in run 1.

sion (30%), whereas the speed of wave propagation is changed by only 2%. In this run, weakly nonlinear theory (the Gardner model) is used to model the solitary wave transformation after the step, as it has been described by Holloway *et al.*,[19] Grimshaw *et al.*,[23] and Maderich *et al.*[24] The coefficients of the Gardner model are calculated using the density ratio and interface position as discussed above in Sec. III. First, we note that only one solitary wave is predicted by this theory[23] for these model parameters and by the numerical modeling. The comparison of the solitary wave shapes obtained by both models is shown in Fig. 4; the solitary wave modeled by the Gardner model is the solid line and the solitary wave modeled by the full nonlinear model is the dashed line. There is no essentially difference in both solitary wave positions during the transformation. The transmitted solitary wave in the framework of the Gardner equation theory has an amplitude of −5.5 cm that is only 7% more than the solitary wave amplitude modeled in the full system of equations (−5.1 cm) but it is a little wider.

This disagreement between the asymptotic theory and the Navier–Stokes model is of the same order as that obtained by Maderich *et al.*[24] for an incident solitary wave of elevation of moderate amplitude and related to a loss of energy in the Navier–Stokes model due small viscosity. The oscillatory tails after the secondary solitary waves are present in both models, but the amplitude of the oscillations in the Navier–Stokes model is smaller than in the asymptotic model. Figure 5 shows the vertical distribution of horizontal velocity in the wave after the step calculated using the Gardner model and the fully nonlinear model. However, the fully nonlinear model predicts more intensive flow in the wave. The maximal difference in horizontal velocity between the Gardner model and the fully nonlinear model is 20%. This difference is related to the continuous stratification in the fully nonlinear model, while the Gardner solitary wave current is determined in the two-layer approximation.

Thus, the process of a depression solitary wave passing over a step agrees quite well with the theoretical scenario of the linear wave transformation at a step and subsequent soliton formation in the transmitted wave field using the Gardner model. There is a surprising result because the nonlinearity of the incident wave characterized by parameter $\varepsilon_{nl}=4$ is quite strong.

B. Run 2

In the next run the amplitude of incident solitary wave at x_r is −8.8 cm, which is less than the limiting value of the solitary wave amplitude in the MCC model (−12 cm). For such amplitudes, the Gardner model is not applicable because the limiting amplitude in this model is only −7.3 cm. The computed shape of the solitary wave is well described by the MCC model (Fig. 6).

The interaction parameter here $\mu=0.44$ and it is bigger than the same parameter in run 1. Although the amplitude of the incident wave in run 2 is only 1.35 times bigger than that in run 1, the process of wave transformation at the step in run 2 differs qualitatively from the process in run 1. As shown in Figs. 7(b) and 7(c), the wave transformation in the vicinity of the step is accompanied by the formation of high-frequency tail.

Let us consider this process in detail using a grid 4800 × 240. Figure 8 shows the transformation of the salinity field during the wave propagation over the step. The wave becomes unstable at its trough and the billows grow at its rear end. The formation of such billows due to KH instability is

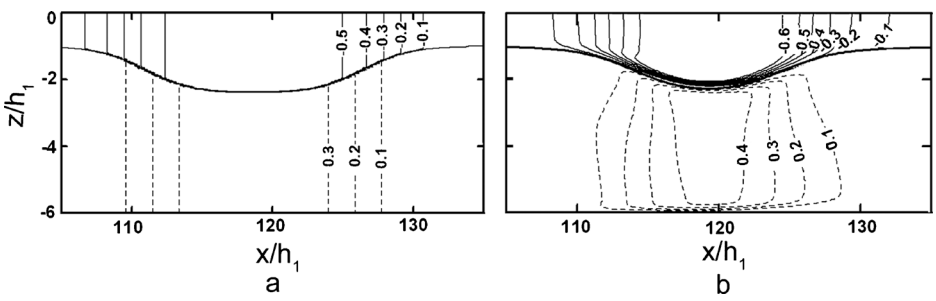

FIG. 5. The comparison of the normalized horizontal velocity U/c_0 in the solitary wave after step at $\tau=505$ in the Gardner model (a) and full nonlinear model (b) in run 1. The interface position is shown by thick line.

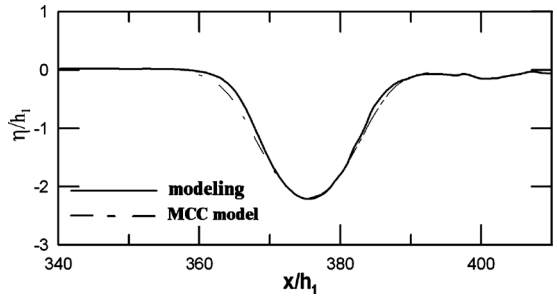

FIG. 6. The comparison of the shape of the incident solitary wave at $\tau = 273$ with the shape of the MCC solitary wave in run 2.

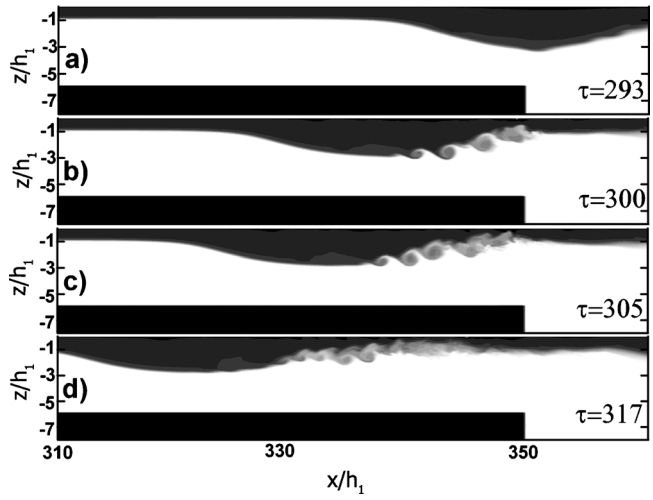

FIG. 8. Development of the KH instability on the wave trough after the step in run 2.

well studied for parallel flows[25–28] and for large-amplitude interfacial waves[29–32] in the basins of constant depth. In the solitary wave trough, the Richardson number is

$$\mathrm{Ri} = -\frac{g}{\rho_0}\frac{\partial \rho}{\partial z}\Big/\left(\frac{\partial U}{\partial z}\right)^2, \tag{15}$$

where U is the horizontal velocity. The thickness of the interface layer is here approximated by a linear distribution of density with $\Delta h = 1.1$ cm. The characteristic scale of the KH billows is about $\lambda_{KH} \approx 8.6$ cm. The vertical structure of the salinity and horizontal velocity and the Richardson number in the wave trough are presented in Fig. 9. In the trough of the solitary wave the interface subsided on the wave amplitude [Fig. 9(a)]. The ratio of the billow scale to the interface thickness $\lambda_{KH}/\Delta h = 7.8$, which agrees well with the estimate[32] $\lambda_{KH}/\Delta h = 7.5$ based on the standard theory for parallel stratified flows,[25,26] and the results of laboratory experiments for an interfacial solitary wave of large amplitude,[32] where $\lambda_{KH}/\Delta h = 7.9$.

The minimum Richardson number in Fig. 9(b) is 0.10. It is less than half the value 0.25 (the boundary for linear stability of parallel stratified flow[25,26]) and agrees quite well with estimations of instability $\mathrm{Ri} < 0.075 \pm 0.035$ and $\mathrm{Ri} < 0.092 \pm 0.016$ for laboratory experiments,[29,32] respectively, and $\mathrm{Ri} < 0.13$ and $\mathrm{Ri} < 0.1$ for numerical experiments,[30,34] respectively. However, the nonuniformity of the flow in the solitary wave suggests that it may be insufficient to use the classical Richardson number as an indicator of instability. Figure 10 shows horizontal velocity distribution and potentially unstable regions ("pockets"[32]) with $\mathrm{Ri} < 0.25$ in the solitary wave before the step, in the wave over the step and in the wave far after the step. As is seen from the figure, the position of pockets coincides with the maximal shear zone. The computations show that minimum values of Ri in these three cases are in the wave troughs and they are 0.22, 0.1, and 0.18, respectively. The horizontal length L_x of pockets with $\mathrm{Ri} < 0.25$ is a helpful predictor of KH instability[32,34] because it characterizes the horizontal extent where unstable

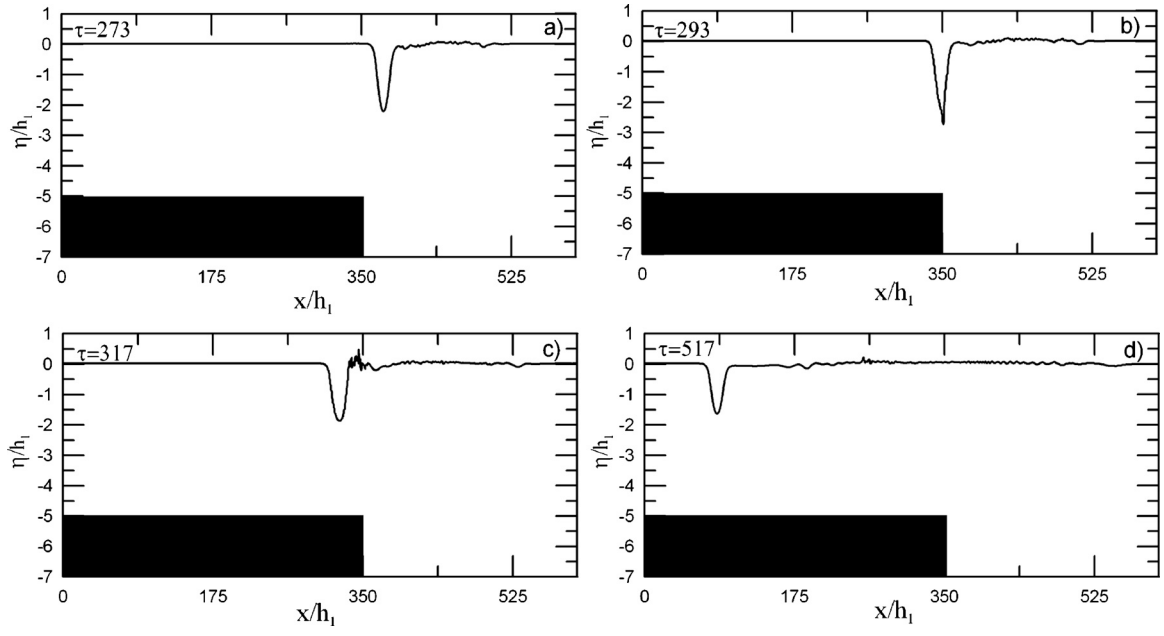

FIG. 7. The solitary wave transformation at the step in run 2 in successive times.

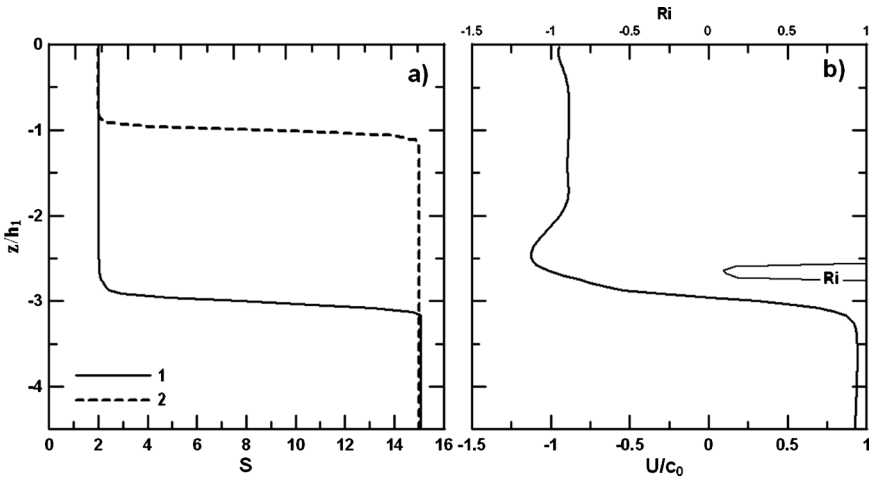

FIG. 9. (a) The comparison of salinity profile at the step as the wave passing (1) and the initial salinity profile (2) and (b) the velocity and the Richardson number profiles at the step as the wave passes in run 2.

motion can grow. The empirical relation $L_x/\lambda_{0.5}=0.86$ suggested by Fructus *et al.*[32] separates potentially stable ($L_x < 0.86\lambda_{0.5}$) and unstable pockets. Here $\lambda_{0.5}$ is the wavelength defined as the width of the solitary wave at the level of the half-amplitude. The computed values $L_x/\lambda_{0.5}$ are 0.76, 1.0, and 0.84 for the pockets shown in Figs. 10(a)–10(c), respectively. So the unstable wave is the wave on the step only, as demonstrated in Fig. 8.

An additional stability criterion for long strongly nonlinear waves in two-layer fluid is available.[33] In the Boussinesq approximation, the equality

$$4a_{cr}^2 - a_{cr}(h_1 - h_2) - h_1 h_2 = 0, \tag{16}$$

yields the critical wave amplitude a_{cr}. The solitary wave is then expected to become unstable for waves with $|a| > |a_{cr}|$. For the pockets shown in Fig. 10, the values $|a_{cr}|$ are equal to 9, 6.9, and 6.9 cm, from (a) to (c), respectively, whereas $|a|=8.8$, 8, and 7.1 cm, respectively. According to this criterion the incoming wave is stable, the wave over the step is unstable, and the wave after the step is slightly unstable, but there is no visible billow formation. As a result, the amplitude of the transmitted wave is decreased due to the KH instability (Fig. 8). This mechanism was parametrized by Bogucki and Garrett[38] in the framework of the Korteweg–de Vries theory. Note that at large Ri, the flow can be unstable to Holmboe modes[39] but it was not observed in our simulations.

When the wave amplitude and shear decreases, the wave is stabilized [Figs. 7(c) and 7(d)] and then transforms into a solitary wave with a dispersive tail [Fig. 7(d)]. The amplitude of the formed solitary wave is about 6.5 cm and its shape is well described by the MCC solution (Fig. 11). Note that the Gardner model predicts a limiting value for the wave amplitude after the step of 5.7 cm, and therefore it cannot describe the transmitted solitary wave.

The reflection coefficient R in run 2 is the same as that in run 1 and is equal to 0.01. Thus, the reflected solitary wave here also has a very small amplitude of about 0.8 cm, and this value is in good agreement with the linear theory.

The results given above are obtained with different grids (2400×120, 4800×240, and 9600×480) and the difference in the results is very small for the description of wave transformation except the fine structure of KH billows. Nevertheless, the ratio of the billow scale to the interface thickness is $\lambda_{KH}/\Delta h \approx 7.8$ for all grids.

C. Run 5

In this run the step height is 16 cm, twice bigger than that used in runs 1 and 2. The initial solitary wave is the same as in run 2 (amplitude −8.8 cm), this shape was reproduced early in Fig. 6. The depth of the lower layer after the step is 12 cm. The interaction parameter μ is 0.74 and the interaction of the incident wave with step is strong in this case. It means that the wave trough goes down very close to the step and we may expect a strong interaction between the wave and the step.

The transformation of this solitary wave at the step is shown in Figs. 12–15. It is clearly evident that wave almost "touches" the step through its trough [Fig. 12(b)]. This leads to the creation of large eddies and consequent strong mixing, as shown in Fig. 15. Due to this the reflection is large and the transmitted wave has a smaller amplitude than in run 2 [cf. Figs. 7(c) and 12(c)]. In linear theory, the reflection coeffi-

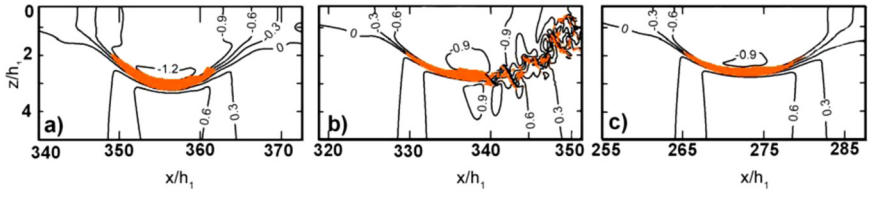

FIG. 10. (Color online) The normalized horizontal velocity U/c_0 and potentially unstable region shown as shaded area where $Ri<0.25$ in solitary wave before step (a), in wave over the step (b), and in wave far after the step (c).

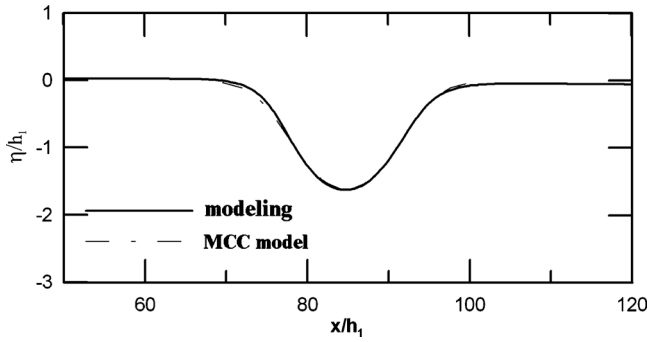

FIG. 11. The comparison of the shape of the transmitted solitary wave at $\tau=517$ with the shape of MCC solitary wave in run 2.

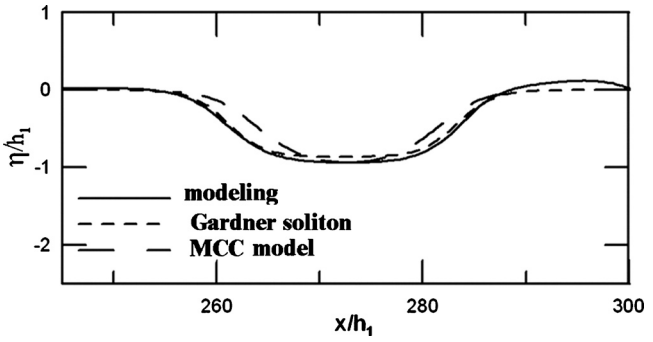

FIG. 13. The comparison of the transmitted wave shape at x_l with the shape of the Gardner and MCC solitary waves in run 5 at $\tau=370$.

cient R here is also small, 0.07. In fact, the reflection is large and the amplitude of the reflected wave is about -4 cm [Fig. 12(c)], which is much larger than Ra_-.

Hence, the linear theory for wave reflection cannot be used for this case. Accordingly, the amplitude of transmitted wave is less than Ta_- ($T=1.04$) and is about -3.5 cm [Fig. 12(c)]. Interestingly, the shape of the transmitted wave at the time $\tau=370$ (Fig. 13) is close to the shape of a table-top solitary wave in both theoretical models but it is not a steady wave and a dispersive tail is generated. At the end of the numerical tank [Fig. 12(d)] the amplitude of the secondary solitary wave is about -2.5 cm and its shape is close to both the Gardner and MCC solitary waves (Fig. 14), and is far from a table-top shape shown in Fig. 13. The wave in Figs. 12(c) and 13 is an example of unsteady thick solitary "formation" which is discussed by Grimshaw *et al.*[40] in connection with the damping of a table-top solitary wave. KH instability is absent in this run 5 due to the strong interaction of the incident wave with the step and the reflection of a large amplitude solitary wave from the step [Fig. 12(c)] that essentially decreases the amplitude of transmitted wave and the shear velocity.

Process of the wave interaction with the bottom step is detailed in Fig. 15 (grid 4800×240). The character of the flow regimes can be characterized by the composite Froude number

$$\mathrm{Fr}^2=\frac{U_1^2}{g'(h_1-\eta)}+\frac{U_2^2}{g'(h_2+\eta)}, \tag{17}$$

where $g'=g\Delta\rho/\rho_0$ and it is shown in Fig. 16.

The interaction process may be divided into several stages. In the first stage [Fig. 15(a)] the front of the incident wave is deformed by flow forming in the lower layer. The Froude number at the step grows to a value 0.4 and the flow is subcritical. In the second and third stages [Figs. 15(b) and 15(c)] this flow becomes critical and supercritical (Fig. 16) at time $\tau=286-291$.

The accelerating countercurrent in the lower layer at the step caused separation of bottom boundary layer and forma-

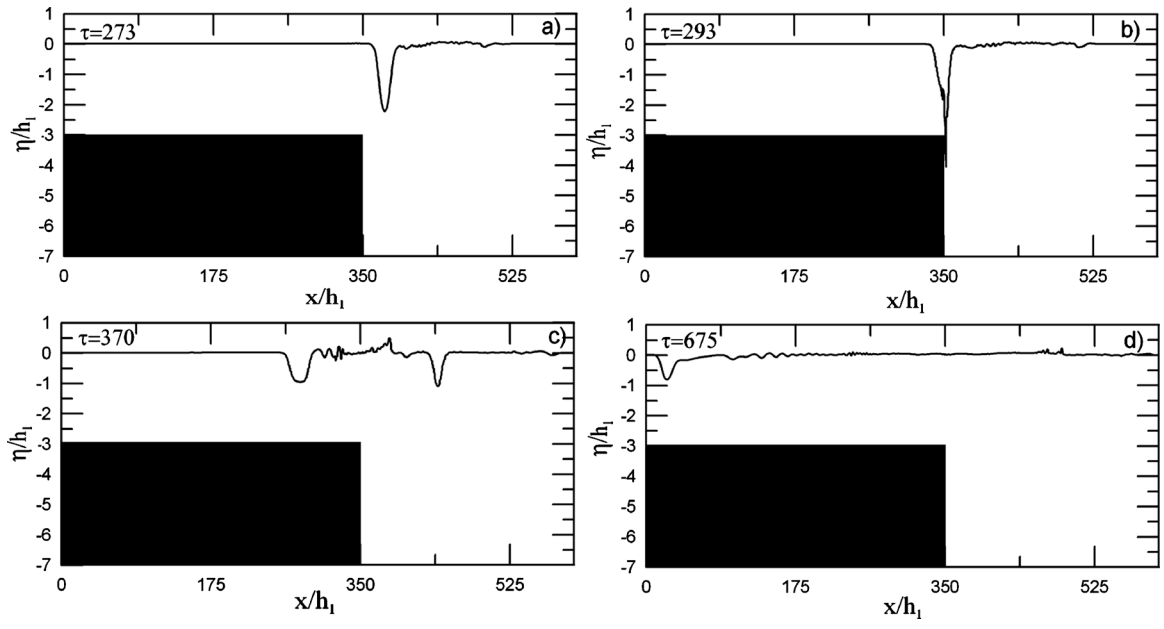

FIG. 12. Solitary wave transformation on the step in run 5 at successive times.

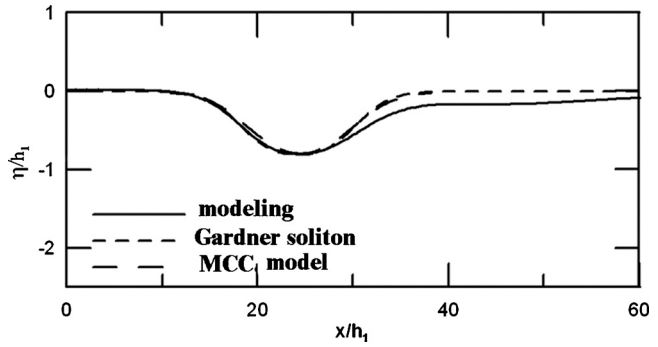

FIG. 14. The comparison of the transmitted wave shape at large distance from the step with the shape of the Gardner and MCC solitary waves in run 5 at $\tau=675$.

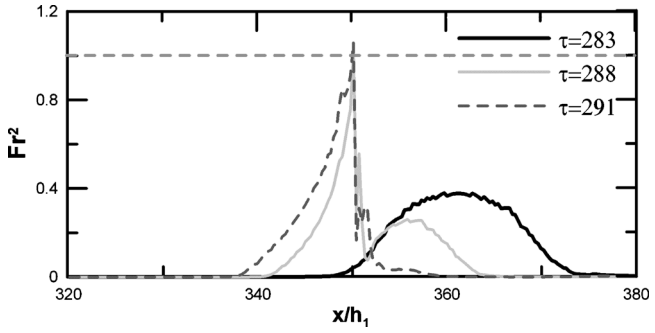

FIG. 16. The composite Froude number of flow at successive times in run 5.

tion of a vortex. This flow entrains the wave trough into the bottom layer, with the formation of a weaker baroclinic eddy of opposite sign above it. This pair of eddies pulls fluid from the upper layer into the lower layer. Then at the fourth stage the pair of eddies reflects from the bottom step, leading to intensive mixing of stratified water in the neighborhood of the step. This numerical modeling agrees qualitatively with the laboratory experiment by Brovchenko *et al.*[37] on the interaction of a solitary wave of large amplitude with long rectangular obstacle.

V. WAVE ENERGY BUDGET

In this section, we describe the energy budget of the transformation of an interfacial solitary wave at a step. The energy density consists of kinetic energy density

$$E_k(x,z,t) = \tfrac{1}{2}\rho_0(U^2 + W^2), \tag{18}$$

where U is the horizontal and W is the vertical velocities, correspondingly, and the potential energy density

$$E_p(x,z,t) = \rho(x,z,t)gz. \tag{19}$$

For estimations of the energy budget transformations, we calculate that part of the potential energy available for conversion into kinetic energy, which may be estimated by the following formula:[41–43]

$$E_a(x,z,t) = g\int_z^{z^*} (\bar{\rho}(z') - \rho)dz', \tag{20}$$

when the reference density $\bar{\rho}(z,t)$ profile is invertible with inverse $z^*(\rho,t)$. In an open system, the undisturbed far field density distribution can be used as a reference profile.[44] However, for a closed basin the reference density $\bar{\rho}(z,t)$ should be obtained by an adiabatic rearranging of the density field. In our case of a very long computational tank, using the undisturbed density distribution leads only to a small difference in the estimation of energy conversion (less that 3%) compared to using the sorting procedure, and hence this simple approach is chosen. The sum of E_k and E_a is called the pseudoenergy density E_{PSE}. When dissipation and diffusion can be ignored and the reference density is time inde-

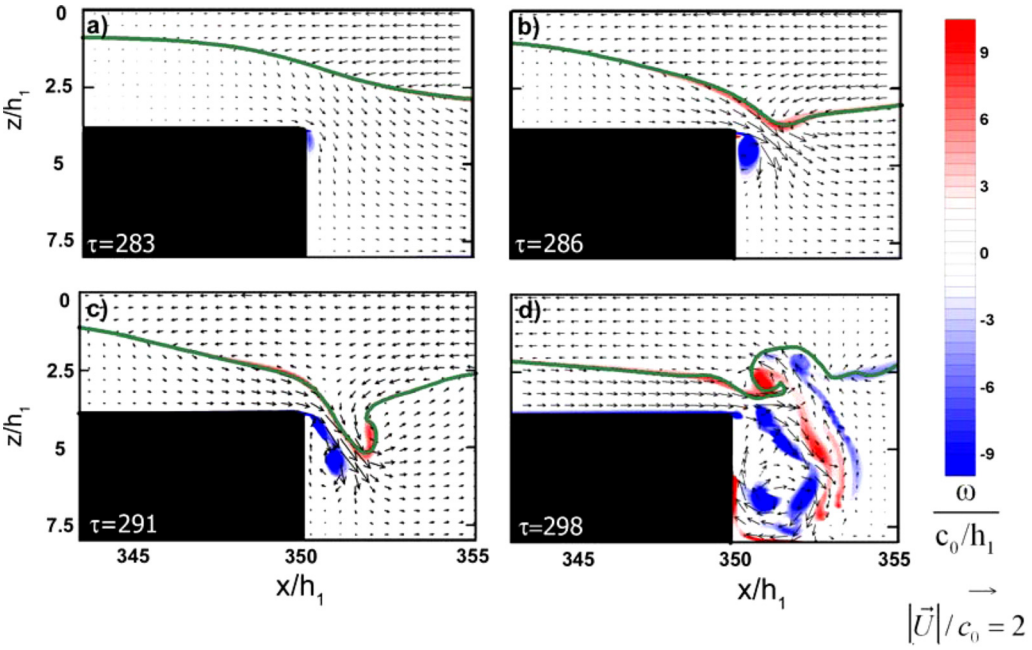

FIG. 15. (Color online) The normalized velocity vectors $\vec{\mathbf{U}}/c_0$ and vorticity $\omega/(c_0 h_1)$ near the step when incident wave passes through it in run 5. The interface position is shown by thick line.

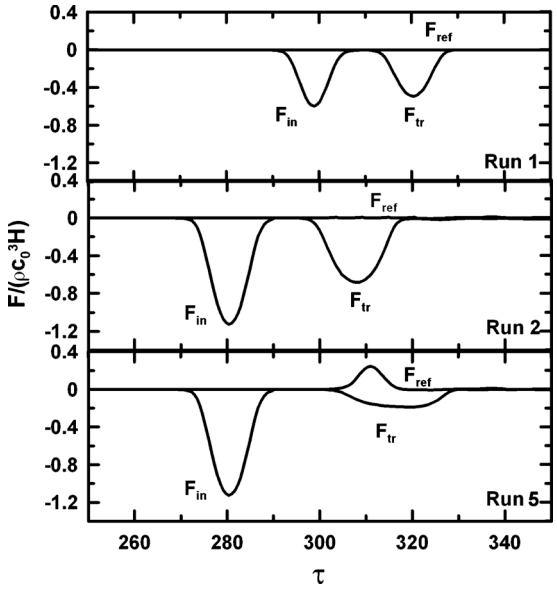

FIG. 17. Pseudoenergy fluxes through the cross section $x_r/h_1=360$ for the incident and the reflected waves and through the cross section $x_l/h_1=330$ for the transmitted wave.

pendent, the evolution of depth integrated pseudoenergy is described by the equation

$$\frac{\partial}{\partial t}\int_{-H}^{0} E_{\mathrm{PSE}}dz + \frac{\partial}{\partial x}F(x,t) = 0, \tag{21}$$

where $F(x,t)$ is the depth integrated pseudoenergy flux

$$F(x,t) = \int_{-H}^{0} (E_{\mathrm{PSE}} + p)Udz, \tag{22}$$

where p is pressure disturbance due to passing wave.

Our goal is to estimate the balance of the total energy after the wave has crossed the step. We estimate the total energy of the incident, reflected, and transmitted waves before the step and after the step by integrating Eq. (21) over the horizontal coordinate x on each side of the step from the tank wall to the positions of the chosen sections shown in Fig. 1. Two sections near the step (before and after it) have been chosen to exclude the zone of mixing at the positions x_r and x_l. We assume that the energy losses take place mainly near the step. The energy fluxes of the incident and reflected waves are estimated at the section x_r and the flux of the transmitted wave is estimated at the section x_l. The energy fluxes $F(x,t)$ for the three described runs are shown in Fig. 17 versus time for the three numerical experiments.

Then volume integration of these flows outside the mixing zone allows us to estimate the energy of the incident ($\mathrm{PSE_{in}}$), reflected ($\mathrm{PSE_{ref}}$), and transmitted ($\mathrm{PSE_{tr}}$) waves, e.g.,

$$\mathrm{PSE_{in}} = \int_{x_r}^{L}\int_{-H}^{0} E_{\mathrm{PSE}}dx = -\int_{t_1}^{t_2} F(x_r,t)dt,$$

$$\mathrm{PSE_{tr}} = \int_{0}^{x_l}\int_{-H}^{0} E_{\mathrm{PSE}}dx = -\int_{t_3}^{t_4} F(x_l,t)dt, \tag{23}$$

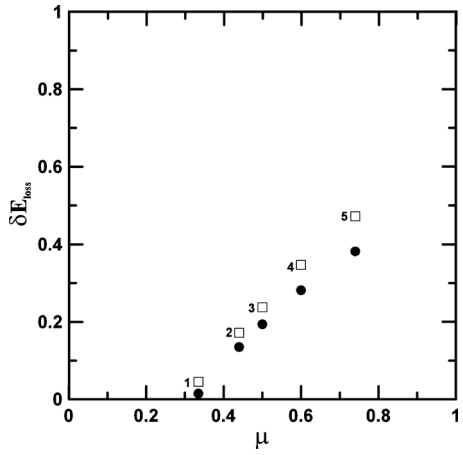

FIG. 18. Loss of the energy due to mixing, turbulence, and dissipation. The squares represent the estimation by Eq. (23) and the black circles correspond to formula (25).

$$\mathrm{PSE_{ref}} = \int_{x_r}^{L}\int_{-H}^{0} E_{\mathrm{PSE}}dx = \int_{t_5}^{t_6} F(x_r,t)dt,$$

where $t_i - t_j$ are the intervals of time when the wave passes the given cross section.

The relative estimation of the energy loss is then given by

$$\delta E_{\mathrm{loss}} = \frac{\mathrm{PSE_{in}} - \mathrm{PSE_{tr}} - \mathrm{PSE_{ref}}}{\mathrm{PSE_{in}}}, \tag{24}$$

and it is plotted versus the interaction parameter $\mu = |a_-|/h_{2+}$ in Fig. 18 for all numerical runs. As seen in figure, the energy loss grows with the increase of the interaction parameter. For the first run, the energy loss is about 5%, and, as has been shown above, the Gardner equation may be used for an approximate description of the transformation of an interfacial solitary wave at the step. For the second and next two runs, the energy losses are 18%, 25%, and 36%, respectively, and for the fifth run, it is 48%. Note that in the framework of weakly nonlinear theory, the estimation of internal solitary wave energy for a two layer-system is given as[45]

$$\mathrm{PSE} = g\Delta\rho\int_{-\infty}^{\infty}\eta^2(x)dx \approx c_0 g\Delta\rho\int_{t_i}^{t_j}\eta^2(x_k,t)dt, \tag{25}$$

where x_k is the position of the cross section. The estimates of δE_{loss} using formula (25) are presented in Fig. 18 and these estimations lie lower than estimates lie below the estimates from the fully nonlinear theory, while the difference between them increases with growth of the interaction parameter. Note that using different grids in run 5 results in a difference in δE_{loss} that does not exceed 3%.

VI. DISCUSSION

In this paper we continue the study of the transformation of an interfacial solitary wave over a bottom step by Grimshaw *et al.*[23] and Maderich *et al.*,[24] using here numerical simulations of the full system of the Navier–Stokes equations for waves of large amplitude. The new effects here are the polarity of the solitary wave, which is now a wave of

depression, large incident wave amplitude, and height of the step. Three fundamentally different scenarios of solitary wave transformation depending on incident wave amplitude and step height are described in detail for the first time. We have also calculated first the total wave energy loss on the step in the range of interaction parameter μ (ratio of wave amplitude to the depth of lower layer on the step). The novel results of this study can be summarized as follows:

(1) Surprisingly, the simulations show the applicability of the weakly nonlinear model (the Gardner equation) to describe even a strongly incident solitary wave ($\varepsilon_{\mathrm{nl}}=4$) transformation over a relatively deep step (interaction parameter $\mu=0.33$) if its amplitude does not exceed the limiting one determined from the Gardner equation. In this case, the predictions of theory by Grimshaw *et al.*[23] agree well with the Gardner model simulations as quite well with numerical simulations into full hydrodynamic equations. The mixing at the step is weak (around 5% of the energy of the incident wave) which allows the use of ideal fluid theories. This case (run 1) can be characterized as a weak interaction.

(2) The second scenario shows that the transformation of an incident solitary wave of amplitude larger than the Gardner soliton limiting amplitude but less than predicted by Miyata–Camassa–Choi theory differs from the previous case totally. The incident wave is stable and its shape is well described by MCC model but it amplitude is larger than the limiting amplitude of an MCC soliton $A_{\mathrm{lim}+}$ after the step ($a_-/A_{\mathrm{lim}+}=1.1$). The following transformation of the transmitted wave after the step is accompanied by shear instability and the formation of KH billows that is typical for the adjustment of large amplitude interfacial solitary waves to a stable state.[13,31,32] The parameters of the billows agree well with theoretical estimates and laboratory measurements.[32] The shape of the transmitted (secondary) solitary wave is described by the MCC model and its amplitude, a_+, is less than the limiting value ($a_+/A_{\mathrm{lim}+}=0.8$). Thus, the KH instability is a new mechanism for the formation of the stable secondary solitary waves from a large amplitude wave passing over the step. The wave reflection is small and the loss of energy of incident wave is 18%. This case (run 2) can be named by a moderate interaction that is characterized moderate value of the interaction parameter $\mu=0.44$.

(3) The third principally different scenario (run 5) is presented for the large height of the step ($h_{2+}/h_{2-}=0.43$) and an incident solitary wave of large amplitude (as in the previous run) when the value of the interaction parameter μ is 0.73. The incident solitary wave undergoes strong reflection from the step and mixing between the layers. This case is classified as a strong interaction. The interaction process can be divided on four stages: (i) the front of incident wave is deformed by flow forming in the lower layer; (ii) the flow becomes hydraulically critical and then supercritical; (iii) this flow entrains the wave trough into the bottom layer, with formation of a strong eddy below the step and a weaker eddy of opposite sign above the step; and (iv) this pair of eddies leads to intensive mixing of the stratified water near the step. About 48% of the energy of the incident wave is lost to dissipation and mixing and 20% of energy is reflected as a solitary wave. Thus, the amplitude of the transmitted wave is less than in run 2. Because of strong interaction, the linear theory for wave reflection cannot be applied to this case. Far from the step, the shape of the secondary solitary wave is well described by both the Gardner and MCC models. However, in the transient phase it is close to the table-top shape that again is described by the Gardner model. We suggest that this solitary wave formation is not a steady solitary wave due to due to its damping in the Navier–Stokes model.

(4) The loss of wave energy at the step is found for all set of runs in range of $0.3<\mu<0.8$. It is shown that in this range the energy loss in the vicinity of the step grows with an increase of the ratio of the incident wave amplitude to the thickness of the lower layer over the step.

ACKNOWLEDGMENTS

The authors thank the support of RFBR Grant Nos. 08-05-91850-KO (T.T., E.P., and R.G.), 09-05-00204 (T.T.), 09-05-90408-SFBR F28.6/010 (V.M., T.T., I.B., and K.T.), and 07-05-92310-HBO_a (T.T. and E.P.)

APPENDIX: MATHEMATICAL MODELING

The numerical model used here is based on the Navier–Stokes equations for a continuously stratified fluid. It was developed by Kanarska and Maderich[46] as a nonhydrostatic extension of the Princeton Ocean Model. The density stratification in the numerical simulations is modeled by salinity stratification. The basic equations are for continuity, momentum, and salinity written in the Boussinesq approximation

$$\nabla\cdot\vec{U}=0 \tag{A1}$$

$$\frac{D\vec{U}}{Dt}=-\frac{1}{\rho_0}\nabla P+\nu\nabla^2\vec{U}-\vec{g}\frac{\rho}{\rho_0}, \tag{A2}$$

$$\frac{DS}{Dt}=\chi\nabla^2 S. \tag{A3}$$

Here, $\vec{U}=(U,V,W)$ is the three-dimensional velocity field in the Cartesian coordinates $\vec{x}=(x,y,z)$, with x directed along the computational flume, y is the transverse coordinate, and z is directed vertically upward; D/Dt is the material derivative; P is the pressure; ρ is density; ρ_0 is undisturbed density; $\vec{g}=(0,0,g)$, g is the gravitational acceleration; S is salinity; and ν and χ are the kinematic viscosity and diffusivity, respectively. Systems (A1)–(A3) are closed by an equation of state[47] for the density ρ of water $\rho=\rho(S,T)$. The numerical solution of these governing equations, with the relevant boundary conditions on the solid boundaries and the free surface, is based on the modified algorithm[46] with a four-stage procedure: (i) computation of the free-surface level and the depth-integrated velocity field; (ii) computation of the provisional hydrostatic components of velocity; (iii) compu-

tation of the nonhydrostatic components of the velocity and pressure fields; and (iv) computation of the scalar fields.

[1]C. J. Amick and R. E. L. Turner, "A global theory of internal solitary waves in two-fluid systems," Trans. Am. Math. Soc. **298**, 431 (1986).
[2]K. K. Tung, T. F. Chan, and T. Kubota, "Large amplitude waves of permanent form," Stud. Appl. Math. **16**, 1 (1982).
[3]T. Kakutani and N. Yamasaki, "Solitary waves on a two-layer fluid," J. Phys. Soc. Jpn. **45**, 674 (1978).
[4]C. G. Koop and G. Butler, "An investigation of internal solitary waves in two-fluid system," J. Fluid Mech. **112**, 225 (1981).
[5]*Environmental Stratified Flows*, edited by R. Grimshaw (Kluwer, Dordrecht, 2001).
[6]E. N. Pelinovsky, A. V. Slunyaev, O. E. Polukhina, and T. G. Talipova, "Internal solitary waves," in *Solitary Waves in Fluids*, edited by R. Grimshaw (WIT, Southampton, 2007), Vol. 85.
[7]M. Miyata, "An internal solitary wave of large amplitude," La Mer **23**, 43 (1985).
[8]M. Miyata, "Long internal waves of large amplitude," in *Proceedings of the IUTAM Symposium on Nonlinear Water Waves*, edited by H. Horikawa and H. Maruo (Springer-Verlag, New York, 1988), p. 399.
[9]W. Choi and R. Camassa, "Fully nonlinear internal waves in a two-fluid system," J. Fluid Mech. **396**, 1 (1999).
[10]L. A. Ostrovsky and J. Grue, "Evolution equations for strongly nonlinear internal waves," Phys. Fluids **15**, 2934 (2003).
[11]K. Lamb and B. Wan, "Conjugate flows and flat solitary waves for a continuously stratified fluid," Phys. Fluids **10**, 2061 (1998).
[12]K. Lamb, "Conjugate flows for a three-layer fluid," Phys. Fluids **12**, 2169 (2000).
[13]J. Grue, A. Jensen, P.-O. Rusas, and J. Sveen, "Properties of large-amplitude internal waves," J. Fluid Mech. **380**, 257 (1999).
[14]M. Stastna and K. Lamb, "Large fully nonlinear internal solitary waves: The effect of background current," Phys. Fluids **14**, 2987 (2002).
[15]V. Vlasenko, N. Stashchuk, and K. Hutter, *Baroclinic Tides* (Cambridge University Press, Cambridge, 2005).
[16]V. D. Djordjevic and L. G. Redekopp, "The fission and disintegration of internal solitary waves moving over two-dimensional topography," J. Phys. Oceanogr. **8**, 1016 (1978).
[17]R. Grimshaw, "Evolution equations for nonlinear internal waves in stratified shear flows," Stud. Appl. Math. **65**, 159 (1981).
[18]P. Holloway, E. Pelinovsky, T. Talipova, and B. Barnes, "Nonlinear model of internal tide transformation on the Australian north west shelf," J. Phys. Oceanogr. **27**, 871 (1997).
[19]P. Holloway, E. Pelinovsky, and T. Talipova, "A generalized Korteweg–de Vries model of internal tide transformation in the coastal zone," J. Geophys. Res. **104**, 18333, doi:10.1029/1999JC900144 (1999).
[20]R. Grimshaw, E. Pelinovsky, T. Talipova, and A. Kurkin, "Simulation of the transformation of internal solitary waves on oceanic shelves," J. Phys. Oceanogr. **34**, 2774 (2004).
[21]R. Grimshaw, E. Pelinovsky, and T. Talipova, "Modelling internal solitary waves in the coastal ocean," Surv. Geophys. **28**, 273 (2007).
[22]V. Vlasenko, L. Ostrovsky, and K. Hutter, "Adiabatic behavior of strongly nonlinear internal solitary waves in slope-shelf areas," J. Geophys. Res. **110**, C04006, doi:10.1029/2004JC002705 (2005).
[23]R. Grimshaw, E. Pelinovsky, and T. Talipova, "Fission of a weakly nonlinear interfacial solitary wave at a step," Geophys. Astrophys. Fluid Dyn. **102**, 179 (2008).
[24]V. Maderich, T. Talipova, R. Grimshaw, E. Pelinovsky, B. H. Choi, I. Brovchenko, K. Terletska, and D. C. Kim, "The transformation of an interfacial solitary wave of elevation at a bottom step," Nonlinear Processes Geophys. **16**, 33 (2009).
[25]L. N. Howard, "Note on a paper by John W. Miles," J. Fluid Mech. **10**, 509 (1961).
[26]J. W. Miles and L. N. Howard, "Note on a heterogeneous shear flow," J. Fluid Mech. **20**, 331 (1964).
[27]W. R. Peltier and C. P. Caulfield, "Mixing efficiency in stratified shear flows," Annu. Rev. Fluid Mech. **35**, 135 (2003).
[28]W. D. Smyth, J. D. Nash, and J. N. Moum, "Differential diffusion in breaking Kelvin–Helmholtz billows," J. Phys. Oceanogr. **35**, 1004 (2005).
[29]C. D. Troy and J. R. Koseff, "The instability and breaking of long internal waves," J. Fluid Mech. **543**, 107 (2005).
[30]O. B. Fringer and R. L. Street, "The dynamics of breaking progressive interfacial waves," J. Fluid Mech. **494**, 319 (2003).
[31]M. Carr, D. Fructus, J. Grue, A. Jensen, and P. A. Davies, "Convectively induced shear instability in large internal solitary waves," Phys. Fluids **20**, 126601 (2008).
[32]D. Fructus, M. Carr, J. Grue, A. Jensen, and P. A. Davies, "Shear induced breaking of large amplitude internal solitary waves," J. Fluid Mech. **620**, 1 (2009).
[33]W. Choi, R. Barros, and T.-C. Jo, "A regularized model for strongly nonlinear internal solitary waves," J. Fluid Mech. **629**, 73 (2009).
[34]M. F. Barad and O. B. Fringer, "Simulations of shear instabilities in interfacial gravity waves," J. Fluid Mech. **644**, 61 (2010).
[35]J. N. Moum, D. M. Farmer, W. D. Smyth, L. Armi, and S. Vagle, "Structure and generation of turbulence at interfaces strained by internal solitary waves propagating shoreward over the continental shelf," J. Phys. Oceanogr. **33**, 2093 (2003).
[36]M. H. Orr and P. C. Mignerey, "Nonlinear internal waves in the South China Sea: Observation of the conversion of depression internal waves to elevation internal waves," J. Geophys. Res. **108**, 3064, doi:10.1029/2001JC001163 (2003).
[37]I. Brovchenko, N. Gorodetskaya, V. Maderich, V. Nikishov, and E. Terletskaya, "Interaction of internal solitary waves of large amplitude with obstacle," Prikladnaya Gidromekhanika (Applied Hydromechanics) **9**, 3 (2007).
[38]D. Bogucki and C. Garrett, "A simple model for the shear-induced decay of an internal solitary wave," J. Phys. Oceanogr. **23**, 1767 (1993).
[39]W. D. Smyth and W. R. Peltier, "Instability and transition in finite amplitude Kelvin-Helmholtz and Holmboe waves," J. Fluid Mech. **228**, 387 (1991).
[40]R. Grimshaw, E. Pelinovsky, and T. Talipova, "Damping of large-amplitude solitary waves," Wave Motion **37**, 351 (2003).
[41]T. G. Shepherd, "A unified theory of available potential-energy," Atmos.-Ocean. **31**, 1 (2006).
[42]A. Scotti, R. Beardsley, and B. Butman, "On the integration of energy and energy fluxes of nonlinear internal waves: An example from Massachusetts Bay," J. Fluid Mech. **561**, 103 (2006).
[43]K. Lamb, "Energy and pseudoenergy flux in the internal wave field generated by tidal flow over topography," Cont. Shelf Res. **27**, 1208 (2007).
[44]K. G. Lamb and V. T. Nguyen, "On calculating energy flux in internal solitary waves with an application to reflectance," J. Phys. Oceanogr. **39**, 559 (2009).
[45]K. R. Helfrich, "Internal solitary wave breaking and run-up on a uniform slope," J. Fluid Mech. **243**, 133 (1992).
[46]Y. Kanarska and V. Maderich, "A non-hydrostatic numerical model for calculating of free-surface stratified flows," Ocean Dyn. **53**, 176 (2003).
[47]G. L. Mellor, "An equation of state for numerical models of ocean and estuaries," J. Atmos. Ocean. Technol. **8**, 609 (1991).